Journal of Molecular Modeling (2023) 29:320
https://doi.org/10.1007/s00894-023-05723-0

ORIGINAL PAPER

The inhibitory mechanism of echinacoside against *Staphylococcus aureus* Ser/Thr phosphatase Stp1 by virtual screening and molecular modeling

Peng Xie[1] · Yue Gao[1] · Chenqi Wu[1] · Xuenan Li[2] · Yanan Yang[1]

Received: 26 June 2023 / Accepted: 9 September 2023 / Published online: 19 September 2023

Abstract

Context Stp1 is a new potential target closely related to the pathogenicity of *Staphylococcus aureus* (*S. aureus*). In this study, effective Stp1 inhibitors were screened via virtual screening and enzyme activity experiments, and the inhibition mechanism was analyzed using molecular dynamics simulation.

Methods AutoDock Vina 4.0 software was used for virtual screening. The molecular structures of Stp1 and ligands were obtained from the RCSB Protein Data Bank and Zinc database, respectively. The molecular dynamics simulation used the Gromacs 4.5.5 software package with the Amberff99sb force field and TIP3P water model. AutoDock Tools was used to add polar hydrogen atoms to Stp1 and distribute part of the charge generated by Kollman's combined atoms. The binding free energies were calculated using the Amber 10 package.

Results The theoretical calculation results are consistent with the experimental results. We found that echinacoside (ECH) substantially inhibits the hydrolytic activity of Stp1. ECH competes with the substrate by binding to the active center of Stp1, resulting in a decrease in Stp1 activity. In addition, Met39, Gly41, Asp120, Asn162, and Ile163 were identified to play key roles in the binding of Stp1 to ECH. The benzene ring of ECH also plays an important role in complex binding. These findings provide a robust foundation for the development of innovative anti-infection drugs.

Keywords Ser/Thr phosphatase · Molecular dynamics simulations · Echinacoside · *Staphylococcus aureus* · Virtual screening

Introduction

Staphylococcus aureus (*S. aureus*) is a common and opportunistic pathogenic bacterium [1] that is widely present in nature. The bacterium can cause infectious diseases [2], including pneumonia, endocarditis, and bacteremia [3], which can lead to death [4]. *S. aureus* frequently causes community and hospital infections [5]. The main drugs used to treat *S. aureus* infections are antibiotics [6]. A methicillin-resistant *S. aureus* strain (MRSA) was first discovered in 1961 [7]. Genomic plasticity and antibiotic abuse have led to increased antibiotic resistance [8]. MRSA isolates are resistant to all available penicillins and other β-lactam antimicrobials [9]. MRSA not only expresses virulence factors [10] but also utilizes a complex mechanism to resist drugs [11]. In 2019, MRSA caused more than 100,000 deaths worldwide in more than 200 countries and regions. Therefore, the development of novel anti-MRSA treatment models is essential.

Currently, proteins related to bacterial growth, drug resistance, and virulence factors have become important targets for combating *S. aureus* [12–15]. Dalal et al. [16] screened three inhibitor molecules of FmtA (ofloxacin, roflumilast, and furazolidone) via virtual screening. Further research revealed that drugs and FmtA can be stably combined, thereby enhancing the thermostability of this protein. Kumari et al. screened five inhibitors that stably bind to ribosome biogenesis GTP-binding (YsxC) via molecular docking [17]. The results demonstrated that inhibitors can be effectively screened using theoretical calculations. In recent years, methods that specifically block

✉ Yanan Yang
18844199768@163.com

[1] Faculty of Food Science and Technology, Suzhou Polytechnic Institute of Agriculture, Suzhou 215008, China

[2] College of Food Science and Engineering, Jilin Agricultural University, Changchun 130118, Jilin, China

bacterial pathogenicity have become a frontier hotspot in research against *S. aureus* infection. This strategy treats bacterial infections by reducing pathogenicity in hosts [18]. Previous research found that serine/threonine kinase/phosphatase (Stk1/Stp1) is involved in regulating the phosphorylation and dephosphorylation of Cys in MgrA and SarA [19] and plays an important role in the regulation of virulence [20]. Stp1 participates in many important pathways, such as bacterial cell wall biosynthesis, virulence factor regulation, and pathways linked with antibiotic sensitivity [21]. Previous studies also showed that after bacteria delete the Stp1 gene, their ability to produce hemolysin is reduced [22]. A murine infection model showed that a Stp1 deletion mutant reduced hepatic abscess formation and tissue necrosis [21], indicating that Stp1 is closely related to the pathogenicity of *S. aureus* and could offer a new target for drug action.

Stp1 belongs to the metal-dependent phosphatase/protein phosphatase 2C (PP2C) family. The structure of Stp1 is similar to those of other PP2C phosphatases [23]. Its core is a β-sandwich consisting of two antiparallel β sheets, which are flanked by a pair of antiparallel helices on either side [22]. The active site is located on top of the β-sandwich and contains four metal ions close to the catalytic site; these ions are responsible for linking water molecules and assist in the catalytic function [23]. Knowledge on the protein structure facilitates further research on drug screening and binding mechanisms.

Echinacoside (ECH) is derived from the herb *Echinacea* species. *Echinacea* is a prominent dietary supplement used worldwide. Caffeic acid derivatives are bioactive compounds of *Echinacea*. Cichoric acid and ECH are important components of caffeic acid derivatives and show major pharmacological properties [24]. Previous studies have shown that ECH exhibits a variety of biological activities, including antioxidative [25], antihyperglycemic [26], anti-inflammatory [27], anticancer [28], and antidepressant [29] activities. However, few studies have investigated the antimicrobial effects of ECH. Via virtual screening, we found that ECH has the potential to inhibit Stp1 activity. Furthermore, phosphatase activity experiments revealed that ECH exhibits the highest inhibitory effect. Subsequently, molecular dynamics simulations and binding free-energy calculations revealed the binding mode of Stp1 and ECH, and fluorescence quenching experiments confirmed these results. This study provides new methods and ideas for the discovery of novel Stp1 inhibitors.

Materials and methods

Bacterial strains and materials

S. aureus strain USA300 was deposited in the laboratory. *Escherichia coli* strains DH5α and BL21 (DE3) were purchased from TIANGEN BIOTECH (Beijing, China) Co., Ltd. Echinacoside was purchased from Chengdu Herbpurify (Chengdu, China) Co., Ltd. Dimethyl sulfoxide (DMSO) was purchased from Sigma–Aldrich (St. Louis, USA).

Plasmid construction, protein expression, and purification

The *S. aureus* USA300 genome was used as the template for PCR [30]. The amplified gene and pET28a vector were digested at 37 °C for 2 h with restriction endonucleases BamHI and XhoI. These two digested fragments were connected with T4 ligase and named PET-28a-Stp1. Construction of the mutant plasmid was performed using a QuikChange™ site-directed mutagenesis kit [31]. After point mutation was performed, the plasmid was digested with DpnI restriction endonuclease and sequenced [32]. The primers used in the experiment are listed in Table 1.

The sequenced plasmid was transfected into BL21 (DE3) cells for expression analysis. The bacteria were cultured in a medium at 37 °C until the $OD_{600\ nm}$ reached 0.5. After adding isopropyl β-D-thiogalactoside to promote the expression of the target protein, the bacteria were cultured at 16 °C overnight. The bacteria were collected by centrifugation and subsequently sonicated. The cell lysate was centrifuged at 12,000 × g for 40 min, and the supernatant was loaded onto a Ni-NTA agarose column [33] that was previously equilibrated with binding buffer (20 mM Tris, pH = 8.0). The column was washed with washing buffer (20 mM Tris, 10 mM imidazole, pH 8.0). After washing, the His-tagged protein was eluted with elution buffer (20 mM Tris, 100 mM imidazole, pH 8.0). The elution solution was concentrated by a Millipore Amicon filter to obtain Stp1 protein.

Virtual screening

AutoDock Vina 4.0 software was used for virtual screening by docking compound to Stp1 [34]. A total of 15,362 natural compounds were obtained from the Zinc database. The 2D structure files of small molecules were converted into 3D structure files that can be used in AutoDock Vina. The 3D

Table 1 Oligonucleotide primers used in this study

Primer name	Oligonucleotide (5′–3′)
Stp1-F	GAAGGATCCATGCTAGAGGCACAATTTTTTAC
Stp1-R	TCTCTCGAGTCATACTTTATCACCTTCAATAG
M39A-F	GTTCTGTGTGATGGTGCGGGTGGCCATAAAG
M39A-R	CTTTATGGCCACCCGCACCATCACACAGAAC
G41A-F	GATGGTATGGGTGCCCATAAAGCAGG
G41A-R	CCTGCTTTATGGGCACCCATACCATC

The modified codons are underlined in each primer sequence

structure of Stp1 was downloaded from the RCSB Protein Data Bank (protein ID:5F1M). AutoDock Tools was used to add polar hydrogen atoms to Stp1 and distribute part of the charge generated by Kollman's combined atoms. Subsequently, a grid box surrounding the hydrolyzed active region was constructed as a ligand docking site. To improve the computational efficiency, the AutoDock Vina search space was minimized to cover the binding site with the following dimensions: center_x = 47.248 Å, center_y = 101.299 Å, and center_z = 195.568 Å; size_x = 14 Å, size_y = 40 Å, and size_z = 16 Å. The ligands were docked individually to the active region of Stp1. The Lamarckian genetic algorithm was used for the entire calculation process during virtual screening [35]. The target protein [36] was always rigid, and all the twisted bonds of the inhibitor could rotate freely [37]. A grid box was created, including metal ions at the active site of the Stp1 receptor, which was positioned on the ligand's center of mass. After each ligand in the ligand library was docked to the active site of Stp1, the binding affinity (kcal/mol) of the ligand-Stp1 system was obtained. Binding affinity is an indicator used to assess the ability of ligands to bind receptor proteins. The values obtained for the binding affinity were sorted from low to high, and the top 50 ligands were selected for structural analysis. Small molecules that are closely bound to the protein activity center and can establish a strong interaction are commonly selected for phosphatase assays.

Phosphatase assay

As described in a previous study [19], the drug was detected using a phosphatase activity assay. The purified Stp1 was preincubated in a 96-well plate with different concentrations of drug in buffer at 25 °C for 10 min. p-Nitrophenyl phosphate (PNPP) was then added to the mixture at a final concentration of 0.8 mM. The samples were incubated for 20 min at 25 °C. The total volume of the mixture was 200 µL. After the reaction was complete, the absorbance was measured at 405 nm using a spectrophotometer. The group containing PNPP and the drug served as the negative control. A group without drug addition was used as a positive control [30]. The absorbance was measured three times at 492 nm after NaOH was added to determine the point at which the reaction was neutralized and completed. Enzyme activity = $(A-A_0)/(A_{100}-A_0) \times 100\%$, where A represents the absorbance of inhibitor groups and A_0 is the negative control measurement. A_{100} was used as a positive control.

Molecular dynamics simulation

The Gromacs 4.5.5 software package with the Amberff99sb force field and TIP3P water model was used for the molecular dynamics simulation [38]. The Stp1 structure file contained Mn^{2+} coordinates. Given that the Amberff99sb force field did not contain the Mn^{2+} force field, the parameters of Mn^{2+} were added to some files (ions.itp, ffnonbonded.itp, and atomtypes.atp) to establish the force field [39]. The initial phase of the Stp1-inhibitor system involved energy relaxation. In this phase, 2000 steps were maximum descending energy minimizations, followed by 2000 steps of conjugate gradient energy minimizations. Subsequently, the temperature and pressure of the system were controlled by 200 ps and 500 ps molecular dynamic runs, while position restriction was applied to the proteins and ligands to allow relaxation of the solvent molecules. Next, a 200 ns MD was run with no position restriction on the solute. The trajectory equilibration was reflected by the balance of various quantities, such as root mean square deviation (RMSD) relative to the initial structure, internal protein energy, and fluctuations calculated at different time intervals. After a 200 ns simulation, the binding energy of the protein and ligand was analyzed using the molecular mechanics/Poisson–Boltzmann surface area (MM/PBSA) method [40]. We evenly selected a total of 100 snapshots from 10 ns on the equilibration MD trajectory at intervals of 100 ps. A detailed description of this method is provided in the Supplementary Materials.

Fluorescence quenching

The binding constants (K_A) of the ligand to the binding site of the wild-type and mutant Stp1 were calculated by fluorescence quenching. Stp1 protein solution (3 mL) and inhibitors were added to a 1 cm quartz cuvette, mixed, and incubated for 10 min. The fluorescence spectra of the mixed solutions were obtained using a fluorescence spectrophotometer. The excitation and emission slits were 5.0 nm, and the excitation wavelength was 280 nm. The calculation expression is $r/Df = n\,K_A - r\,K_A$ [41], where r is the amount of ligand per mol of protein-bound material ($r \approx \Delta F/F_0$), Df is the free concentration of quercetin, and n refers to the quantity of binding sites.

Bioinformatics prediction

The SwissADME program (http://www.swissadme.ch) from the Swiss Institute of Bioinformatics can predict the absorption, distribution, metabolism, excretion (ADME), and pharmacokinetic properties of drugs [42]. Accessing http://www.swissadme.ch in a web browser directly displays the submission page of SwissADME. The structure of the ligand was entered, and the analysis result was obtained. The software reveals molecular properties from physicochemical properties, pharmacokinetics, and medicinal chemistry friendliness.

Results and discussion

ECH inhibits Stp1 activity

Using virtual screening, we found that ECH (Fig. 1a) has the potential to inhibit Stp1. Therefore, phosphatase activity was measured using Stp1 at different drug concentrations. The results showed that ECH strongly inhibited Stp1 activity (Fig. 1b). As the drug concentration increased, the activity of Stp1 gradually decreased. At an ECH concentration of 2 μg/mL, the inhibition rate was 16.00%. When the ECH concentration was 16 μg/mL, the degree of inhibition exceeded 50%.

To further study the mechanism by which ECH inhibits Stp1, enzyme kinetic assays were carried out. As shown in Fig. 2, the K_M values in the reaction changed. Therefore, we conclude that ECH is a competitive inhibitor of Stp1.

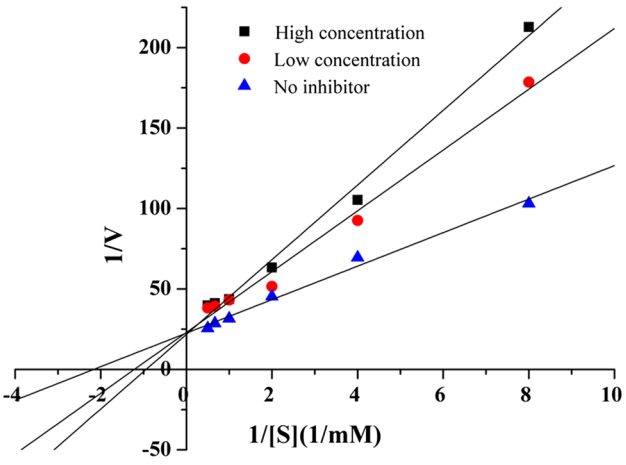

Fig. 2 Lineweaver–Burk plot of Stp1 activity against different concentrations of ECH indicates that ECH is a competitive inhibitor

Virtual screening analysis

To screen the potential inhibitors of Stp1, Stp1 and the ligands were docked to obtain the binding affinity [43]. According to previous reports, verbascoside (VBS) exerts a significant inhibitory effect on Stp1 by binding to the active site of Stp1 [30]. Molecular docking experiments found that the binding affinity of Stp1-VBS was 7.4 kcal/mol, which was used as the cutoff value to select the active compound. According to the binding affinity, the top 50 ligands were selected. As previously mentioned, small molecules that were closely bound to the protein activity center and could establish a strong interaction were selected by the PyMOL and LigPlus software [33]. Therefore, these candidate compounds showed the potential to become an inhibitor of Stp1 [13]. Subsequently, a total of nine molecules were selected as candidate compounds, and enzyme activity experiments were conducted to verify their inhibitory activity (Table 2). The docking results are shown in Fig. 3. Enzyme activity experiments showed that ECH exhibits a significant inhibitory effect on Stp1.

Determination of the binding mode of Stp1 with ECH

In this study, the potential binding mode of the Stp1-ECH complex was determined using molecular docking, molecular dynamics simulations, and binding free energy calculations. According to the results of the virtual screening and activity experiment, ECH can bind to the active site of Stp1 and effectively inhibit the hydrolytic activity of Stp1. A three-dimensional structure of the Stp1-ECH complex obtained by molecular docking was used as the initial coordinates for the molecular dynamics simulations. Based on the molecular docking results, a 200 ns molecular dynamics

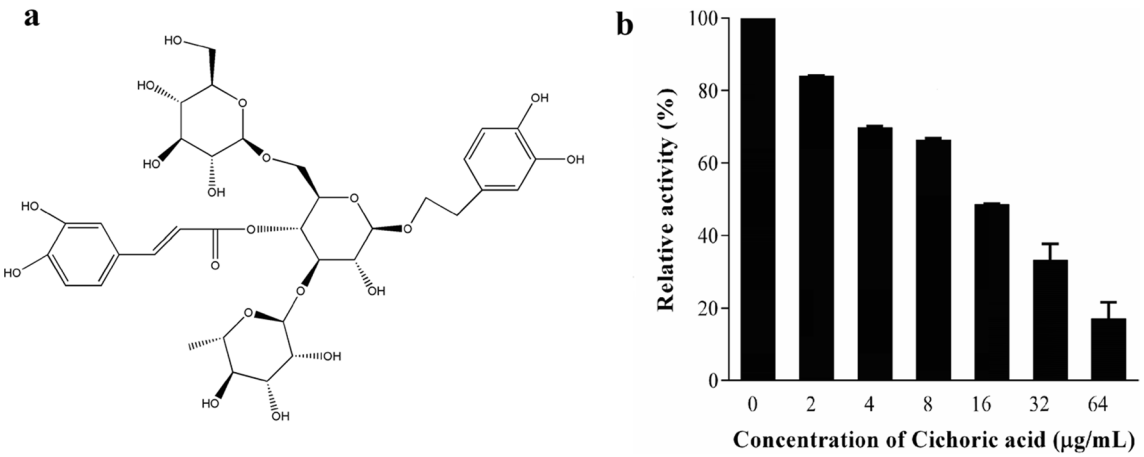

Fig. 1 Inhibition of Stp1 by ECH. **a** Structure of ECH. **b** Inhibitory effect of ECH on Stp1

Table 2 Binding affinity and inhibition ratio of 9 candidate compounds

No.	Ligands	Name	Binding affinity (kcal/mol)	IC_{50} (μg/mL)
1	ZINC4273446	Hawthorn acid	−9.4	>64
2	ZINC4175638	Quercetin	−9.1	N/A[a]
3	ZINC338122	Jatrorrhizin	−8.7	N/A
4	ZINC169724091	Vaccarin	−8.4	N/A
5	ZINC39111	Fisetin	−8.4	N/A
6	ZINC169345514	Hydroxysafflor yellow A	−8.1	N/A
7	ZINC95613012	Echinacoside	−7.7	23.12
8	ZINC169721173	Epmedin C	−7.6	N/A
9	ZINC299810059	Rebaudioside A	−7.6	N/A

[a]The drug has no inhibitory activity at a concentration of 100 μg/mL

simulation of the Stp1-ECH complex was conducted to explore the underlying mechanism. The RMSD is an important indicator for analyzing the structural stability of complexes [16]. To investigate the stability of the complex system during the simulation [12], the RMSD values of the complex and free proteins during a 200 ns simulation were calculated (Fig. 4a). The RMSD values of the Stp1-ECH complex (~ 0.28 nm) and ECH (~ 0.12 nm) were smaller than that of free Stp1. Therefore, the combination of Stp1 and ECH was more stable. After 25 ns, the RMSD value of the system stabilized. Therefore, the complex system reached equilibrium during the 180–200 ns simulation, and the trajectory of the molecular dynamics simulation could be used for subsequent analysis. After a 200 ns molecular dynamics simulation, the stable binding mode of the ECH and Stp1 complex system was obtained. ECH bonded to the active region of Stp1 via hydrogen bonding and hydrophobic interactions (Fig. 4b). ECH, especially the benzene ring, was tightly bound by Met39, Gly41, Asp120, Asn162, and Ile163 of Stp1, as shown in Fig. 4b. The side chains of Met39 and the carbonyl group of Asn162 tightly bonded the benzene ring of ECH at the binding site. The carboxyl group of Asp 120 strongly interacted with the phenolic hydroxyl group of ECH. As revealed by PyMOL software, compared to other inactive site amino acids, Gly41 and Ile163 were closer to ECH; thus, these two amino acids and the drug may interact.

Table 3 shows that the Stp1-VBS complex exhibited negative van der Waals (~ −26.32 kcal/mol), electrostatic (~ −23.75 kcal/mol), and SASA (~ −3.75 kcal/mol) energies, resulting in a total binding energy of −16.63 kcal/mol. Compared with Stp1-VBS, the Stp1-ECH complex exhibits a lower binding energy. Therefore, the combination of Stp1 and ECH is more stable.

The root mean square fluctuation (RMSF) reflects the fluctuation in each residue and reveals the flexibility of the system [44]. The average RMSF values of Stp1-ECH and free Stp1 were 0.10 and 0.13 nm, respectively. Compared with the free protein, the binding site residues in the complex system exhibited a smaller RMSF value, indicating that the residues of the binding site in the complex system were less flexible (Fig. S1). These residues became more rigid due to binding with ECH. The radius of gyration (Rg) was used to characterize the compactness of the complex. As seen in Fig. S2, the Rg of ECH-Stp1 is lower than that of free Stp1, which is consistent with previous results.

Confirmation of the binding mode of ECH to Stp1

To further analyze the interaction between ECH and Stp1, we applied the MM/PBSA method to calculate the electrostatic (ΔE_{ele}), van der Waals (ΔE_{vdw}), solvation (ΔE_{sol}), and total contribution (ΔE_{total}) of the residues to the binding free energy. As shown in Fig. 5, most of the decomposed energy interactions originated from van der Waals forces, which resulted from the strong hydrophobic interactions between the protein and ligand.

As shown in Fig. 5, Ile163 exhibited significant van der Waals contributions (~ −2.43 kcal/mol), resulting in binding energy contributions of −2.76 kcal/mol. This indicates that Ile163 and ECH exhibit a strong hydrophobic interaction. In addition, Met39 and Gly41 exhibited electrostatic (~ −0.63 and −0.07 kcal/mol), van der Waals (~ −1.78 and −0.83 kcal/mol), and solvation (~ −0.12 and −0.01 kcal/mol) force contributions, resulting in strong binding free energy contributions (−2.53 and −0.91 kcal/mol). This was primarily attributed to the strong hydrophobic interaction between Met39 and Gly41 with the benzene ring of ECH. Although the van der Waals and solvation forces were unfavorable, Asp120 provided a strong electrostatic contribution, resulting in a ΔE_{total} value of −1.19 kcal/mol. This indicates that hydrogen bonds could form between Asp120 and ECH. In addition, Asn162 provided significant van der Waals and electrostatic contributions, resulting in binding energy contributions of −1.38 kcal/mol. Therefore, hydrophobic interactions occurred between Asn162 with ECH due to strong hydrogen bonding between Asn162 and ECH.

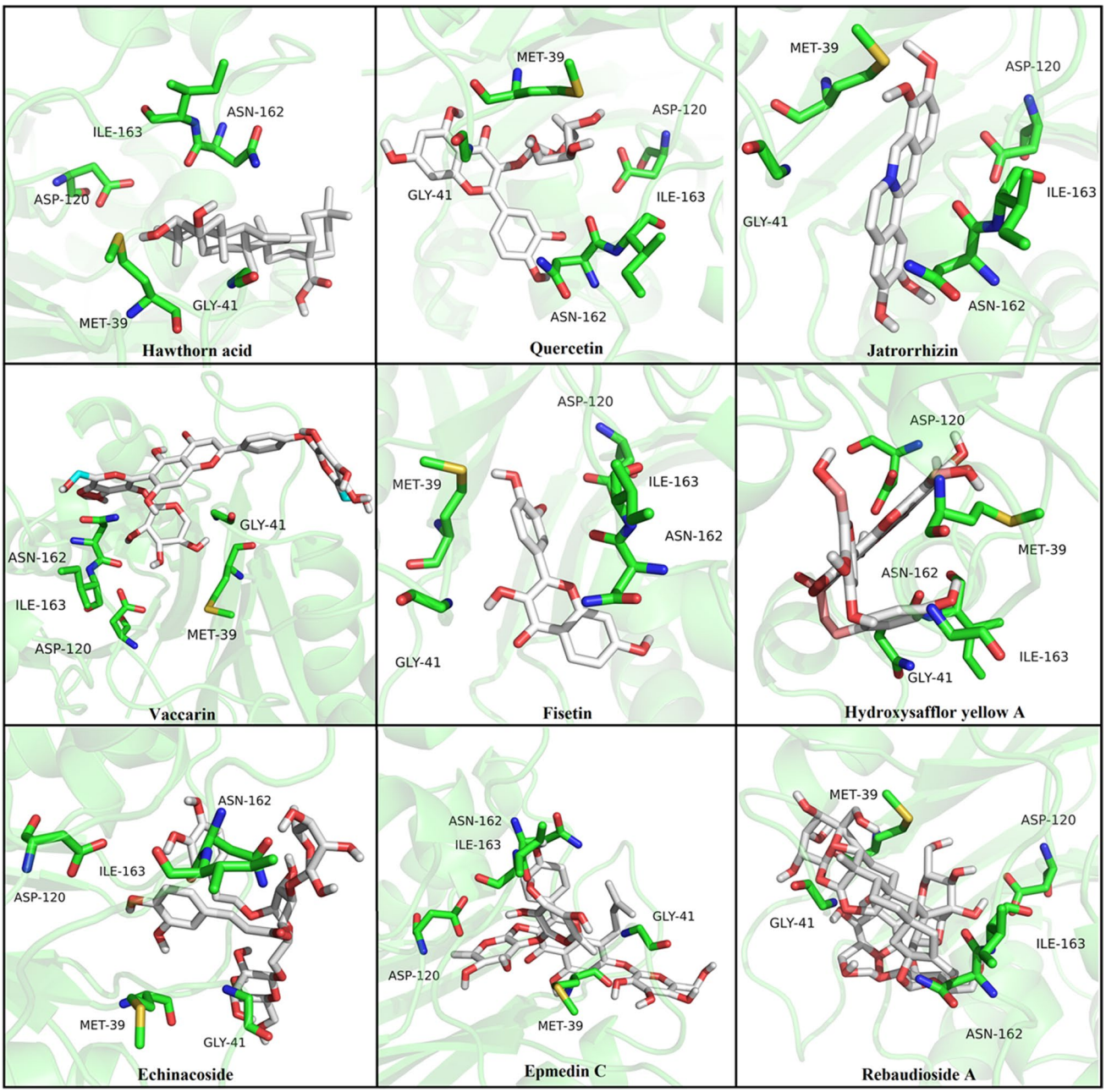

Fig. 3 Ligand binding poses at the active site of Stp1

Decomposition of the binding free energy further indicated that the amino acid residues in the binding site of Stp1 to ECH were Met39, Gly41, Asp120, Asn162, and Ile163.

Hydrogen bonding is a strong interaction that plays an important role in the stability of protein–ligand complexes [17]. To further study hydrogen bonding between Stp1 and its ligands, the number of hydrogen bonds was determined using a trajectory file. As shown in Fig. 6a, the number of hydrogen bonds fluctuated between four and five during the simulation, suggesting that the ligand formed four or five hydrogen bonds with the amino acid residues of Stp1. As shown in Fig. 6b, according to the LigPlus software, ECH can form four strong hydrogen bond interactions with the amino acid residues of proteins, which confirms the above conclusion. Stp1 and VBS can directly form a stable hydrogen bond [30], and there are more hydrogen bonds in the Stp1-ECH complex than the Stp1-VBS complex.

The distance between the ligand ECH and the amino acid of Stp1 was also calculated and analyzed. As shown in Fig. 7, the distances between the inhibitor ECH and the

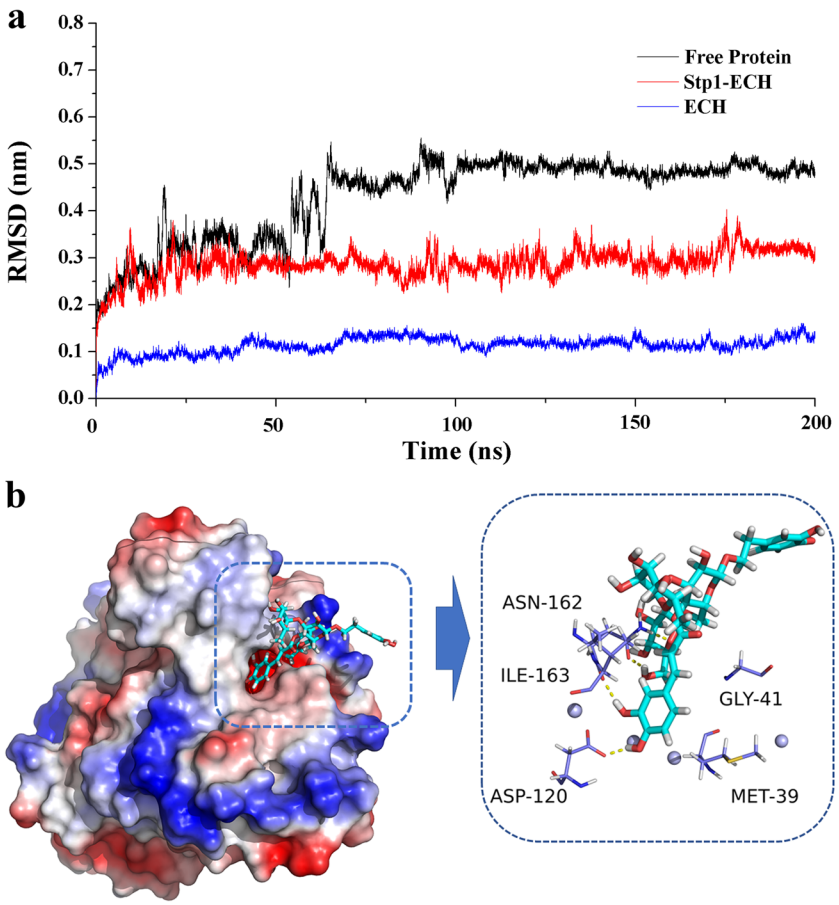

Fig. 4 This paper demonstrates the potently competitive binding mode of Stp1 and ECH through molecular modeling. **a** RMSD plot of free protein, Stp1-ECH, and ECH in 200 ns. **b** Stable three-dimensional (3D) structure of Stp1 binding with ECH based on MD simulation. The hydrogen-bonding interactions are shown as yellow dashed lines

Table 3 Binding free energies (kcal/mol) between Stp1 and compounds by the MM/PBSA method

Compound	van der Waals energy	Electrostatic energy	Polar solvation energy	SASA energy	Binding energy
VBS	−26.32	−23.75	37.19	−3.75	−16.63
ECH	−30.40	−85.37	103.63	−5.89	−18.03

binding site amino acids were less than 0.2 nm, further indicating that ECH interacts strongly with amino acids Met39, Gly41, Asp120, Asn162, and Ile163. According to previous reports [45], these amino acids are located in the active region of Stp1. Therefore, ECH inhibits the hydrolytic activity of Stp1 via competitive inhibition.

Identification of the binding mode of ECH and Stp1

To verify the theoretical calculation results, the Met39 and Gly41 residues of Stp1 were mutated to alanine (Ala) to obtain mutants M39A-Stp1 and G41A-Stp1, respectively. After protein expression and purification, the mutant protein was obtained and used for subsequent phosphatase hydrolysis and fluorescence quenching experiments. The binding constants (K_A) of ECH and Stp1 were calculated by the fluorescence quenching method. The binding constants (K_A) of the WT-Stp1-ECH, M39A-ECH, and G41A-ECH systems were 7.76, 2.81, and 5.73 × 10^5 L/mol, respectively. The binding affinity of the mutant decreased compared to the wild-type, resulting in the following binding order: WT-Stp1 > G41A-Stp1> M39A-Stp1. This indicates that the wild-type protein was the most suitable to bind to ECH.

As shown in Fig. 8, the phosphatase assays revealed that the inhibitory activity of ECH on mutant Stp1 was lower than that on WT-Stp1. Therefore, the mutation of the two amino acid residues, namely, Met39 and Gly41, directly reduced the inhibitory ability of ECH. Mutating the binding site residues reduced the binding affinity of the inhibitor to Stp1, thus resulting in loss of inhibitory activity. Therefore, the experimental results further verified that a reliable complex structure was produced by molecular dynamics simulations.

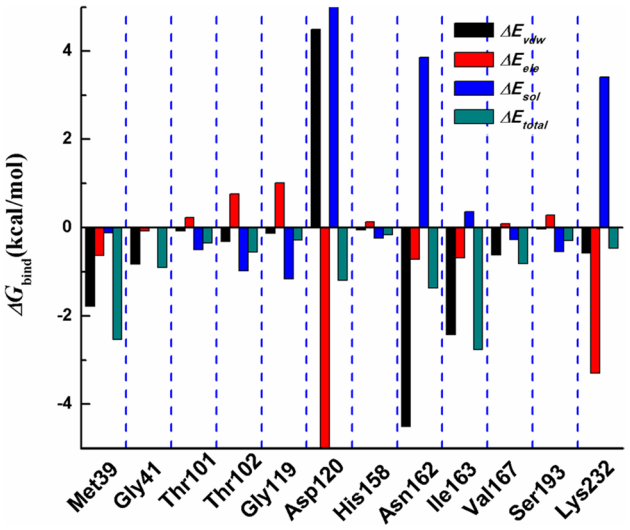

Fig. 5 Decomposed binding free energies of the residues in the binding site. The histogram chart shows the van der Waals (black), electrostatic (red), solvation (blue), and total (green) contributions for the complexes

Lipinski and ADMET properties of ECH

The SwissADME software can predict Lipinski and ADME based on a molecular structure. Given that the values of fraction Csp3 (Fraction Csp3 = 0.57) and log *S* (ESOL) (log *S* = −2.63) were within the standard value range, the solubility and saturation of ECH were adequate. Therefore, ECH can be easily dissolved and formulated, which is conducive to absorption. Conversely, the Log $P_{o/w}$ values were not within the standard range, and the saturation was poor. Based on pharmacokinetic studies, the gastrointestinal absorption of ECH was low. However, ECH can pass through the blood–brain barrier in permanent middle cerebral artery occlusion in rats [46].

According to Lipinski's rule, ECH is not suitable for oral administration due to the relative molecular mass and the number of hydrogen bond receptors, which exceeds the standard. The prediction results are consistent with previous experimental studies. Utilizing absorption promoters and new formulation technologies can improve bioavailability. Li et al. formulated ECH into a phospholipid complex to enhance its bioavailability [47]. Shen et al. used verapamil and clove oil to enhance the intestinal absorption and oral bioavailability of ECH [48].

Moreover, ECH is a natural compound. The medicinal history of plants rich in ECH shows that its adverse reactions and toxic effects are relatively minor. Animal and cell experiments have shown that ECH exhibits good activity in the treatment of osteoporosis [49] and liver injury [50]. ECH can be employed to develop new anti-infective drugs using nano-based drug delivery systems.

Conclusions

ECH is a natural compound with numerous biological activities. In this study, using virtual screening and enzyme activity assays, we found that ECH is a novel Stp1 inhibitor. Further studies showed that ECH binds to the active center of Stp1, preventing binding to Stp1 by

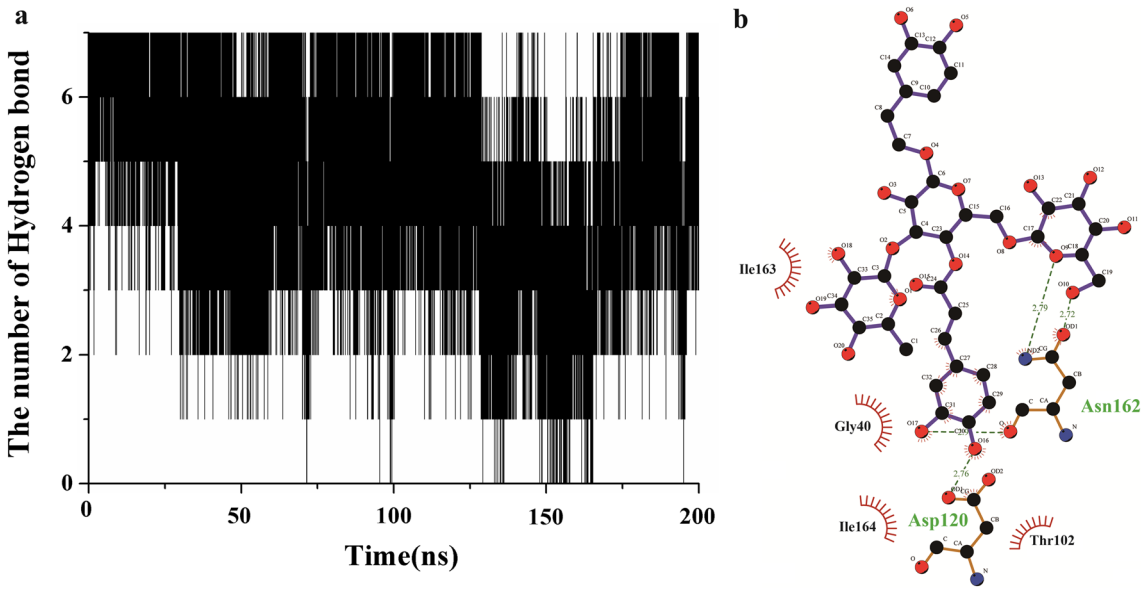

Fig. 6 Interaction between ECH and Stp1 demonstrated in the competitive binding mode. **a** Number of hydrogen bonds between ECH and Stp1. **b** Interaction between ECH and the residues of binding sites of Stp1 identified using LigPlus software

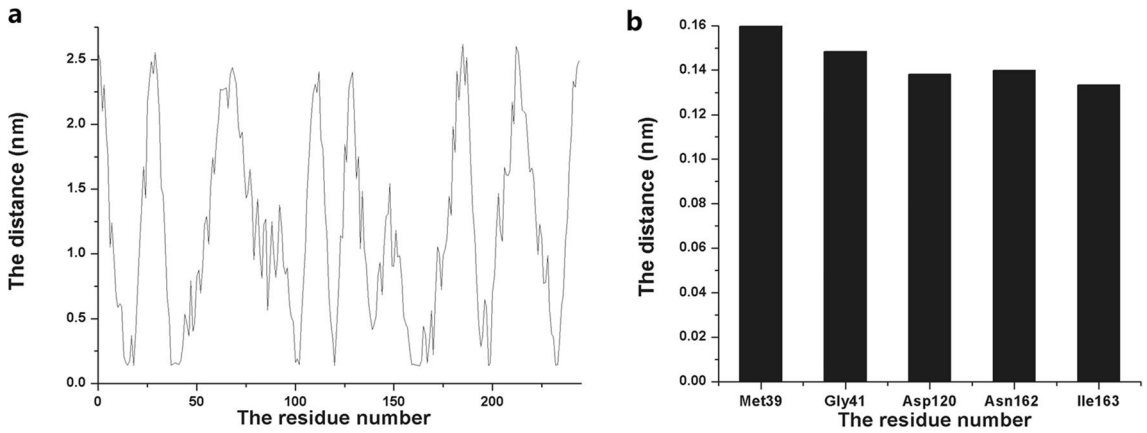

Fig. 7 **a** Distance between all residues of Stp1 and ECH. **b** Distances between the residues in the binding sites of Stp1 and ECH

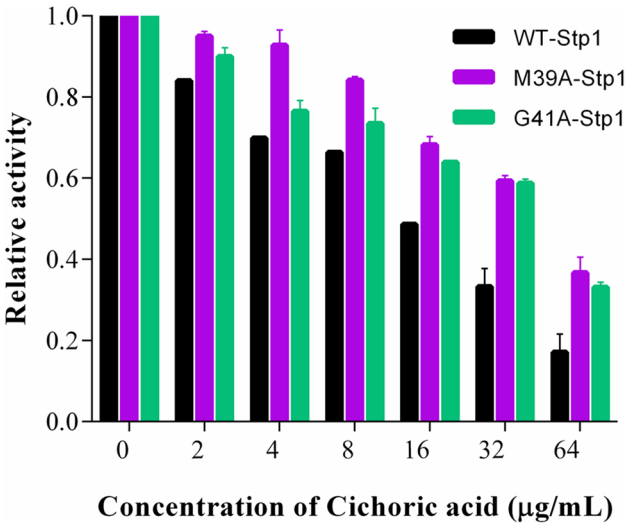

Fig. 8 Enzyme inhibition assays of ECH against wild-type-Stp1, M39A-Stp1, and G41A-Stp1

substrate competition and thus reducing enzyme activity. This was mainly due to residues Met39, Gly41, Asp120, Asn162, and Ile163 of Stp1. The benzene ring of ECH also plays an important role in complex binding. These results provide information useful for the design and development of antimicrobial drugs targeting *S. aureus* and will thus be useful for the discovery and design of new Stp1 inhibitors.

Supplementary Information The online version contains supplementary material available at https://doi.org/10.1007/s00894-023-05723-0.

Author contribution Peng Xie: conceptualization, methodology, funding acquisition, and writing—original draft. Yue Gao: data curation, validation, investigation, and resources. Chenqi Wu: formal analysis, conceptualization, and methodology. Xuenan Li: investigation, software, and data curation. Yanan Yang: funding acquisition, supervision, and writing—review and editing.

Funding This work was sponsored by Qing Lan Project of Jiangsu Province in 2023 and the Doctoral Promotion Program Research Initiation Fund of Suzhou Polytechnic Institute of Agriculture (grant no. BS[2022]21).

Data availability The datasets generated during and/or analyzed during the current study are available from the corresponding author on reasonable request.

Declarations

Conflict of interest The authors declare no competing interests.

References

1. Ronco T, Stegger M, Pedersen K (2017) Draft genome sequence of a sequence type 398 methicillin-resistant *Staphylococcus aureus* isolate from a Danish dairy cow with mastitis. Microbiol Resour Announc 5:1–2. https://doi.org/10.1128/genomeA.00492-17
2. Cuny C, Witte W (2017) MRSA in equine hospitals and its significance for infections in humans. Vet Microbiol 200:59–64. https://doi.org/10.1016/j.vetmic.2016.01.013
3. Paterson GK, Harrison EM, Holmes MA (2014) The emergence of mecC methicillin-resistant *Staphylococcus aureus*. Trends Microbiol 22:42–47. https://doi.org/10.1016/j.tim.2013.11.003
4. Sidairi HA, Reid EK, LeBlanc JJ, Sandila N, Head J, Davis I, Bonnar P (2023) Optimizing treatment of *Staphylococcus aureus* Bloodstream infections following rapid molecular diagnostic testing and an antimicrobial stewardship program intervention. Microbiol Spectr 19:1592–1601. https://doi.org/10.1128/spectrum.01648-22
5. Kumar G, Kiran Tudu A (2023) Tackling multidrug-resistant *Staphylococcus aureus* by natural products and their analogues acting as NorA efflux pump inhibitors. Bioorg Med Chem 80:1–20. https://doi.org/10.1016/j.bmc.2023.117187
6. Li B, Webster TJ (2018) Bacteria antibiotic resistance: new challenges and opportunities for implant-associated orthopedic infections. J Orthop Res 36:22–32. https://doi.org/10.1002/jor.23656
7. Becker K, van Alen S, Idelevich EA, Schleimer N, Seggewiss J, Mellmann A, Kaspar U, Peters G (2018) Plasmid-encoded transferable mecB-mediated methicillin resistance in *Staphylococcus*

aureus. Emerg Infect Dis 24:242–248. https://doi.org/10.3201/eid2402.171074
8. Pichon C, Felden B (2005) Small RNA genes expressed from *Staphylococcus aureus* genomic and pathogenicity islands with specific expression among pathogenic strains. Proc Natl Acad Sci USA 102:14249–14254. https://doi.org/10.1073/pnas.0503838102
9. David MZ, Daum RS (2010) Community-associated methicillin-resistant *Staphylococcus aureus*: epidemiology and clinical consequences of an emerging epidemic. Clin Microbiol Rev 23:616–687. https://doi.org/10.1128/CMR.00081-09
10. Scherr TD, Roux CM, Hanke ML, Angle A, Dunman PM, Kielian T (2013) Global transcriptome analysis of *Staphylococcus aureus* biofilms in response to innate immune cells. Infect Immun 81:4363–4376. https://doi.org/10.1128/iai.00819-13
11. Shore AC, Deasy EC, Slickers P, Brennan G, O'Connell B, Monecke S, Ehricht R, Coleman DC (2011) Detection of *Staphylococcal* cassette chromosome mec Type XI carrying highly divergent mecA, mecI, mecR1, blaZ, and ccr genes in human clinical isolates of clonal complex 130 methicillin-resistant Staphylococcus aureus. Antimicrob Agents Chemother 55:3765–3773. https://doi.org/10.1128/aac.00187-11
12. Dalal V, Kumari R (2022) Screening and identification of natural product-like compounds as potential antibacterial agents targeting FemC of *Staphylococcus aureus*: an in-silico approach. ChemistrySelect 7:1–9. https://doi.org/10.1002/slct.202201728
13. Kumari R, Dalal V (2022) Identification of potential inhibitors for LLM of *Staphylococcus aureus*: structure-based pharmacophore modeling, molecular dynamics, and binding free energy studies. J Biomol Struct Dyn 40:9833–9847. https://doi.org/10.1080/07391102.2021.1936179
14. Dalal V, Golemi-Kotra D, Kumar P (2022) Quantum mechanics/molecular mechanics studies on the catalytic mechanism of a novel esterase (FmtA) of *Staphylococcus aureus*. J Chem Inf Model 62:2409–2420. https://doi.org/10.1021/acs.jcim.2c00057
15. Dalal V, Kumar P, Rakhaminov G, Qamar A, Fan X, Hunter H, Tomar S, Golemi-Kotra D, Kumar P (2019) Repurposing an ancient protein core structure: structural studies on FmtA, a novel esterase of *Staphylococcus aureus*. J Mol Biol 431:3107–3123. https://doi.org/10.1016/j.jmb.2019.06.019
16. Dalal V, Dhankhar P, Singh V, Singh V, Rakhaminov G, Golemi-Kotra D, Kumar P (2021) Structure-based identification of potential drugs against FmtA of *Staphylococcus aureus*: virtual screening, molecular dynamics, MM-GBSA, and QM/MM. Protein J 40:148–165. https://doi.org/10.1007/s10930-020-09953-6
17. Kumari R, Rathi R, Pathak SR, Dalal V (2022) Structural-based virtual screening and identification of novel potent antimicrobial compounds against YsxC of *Staphylococcus aureus*. J Mol Struct 1255:1–11. https://doi.org/10.1016/j.molstruc.2022.132476
18. Chen F, Di H, Wang Y, Cao Q, Xu B, Zhang X, Yang N, Liu G, Yang CG, Xu Y, Jiang H, Lian F, Zhang N, Li J, Lan L (2016) Small-molecule targeting of a diapophytoene desaturase inhibits *S. aureus* virulence. Nat Chem Biol 12:174–179. https://doi.org/10.1038/nchembio.2003
19. Zheng W, Liang Y, Zhao H, Zhang J, Li Z (2015) 5,5 ′-Methylenedisalicylic acid (MDSA) modulates SarA/MgrA phosphorylation by targeting Ser/Thr phosphatase Stp1. Chembiochem 16:1035–1040. https://doi.org/10.1002/cbic.201500003
20. Burnside K, Lembo A, Harrell MI, Gurney M, Xue L, Nguyen-Thao Binh T, Connelly JE, Jewell KA, Schmidt BZ, de los Reyes M, Tao WA, Doran KS, Rajagopal L (2011) Serine/threonine phosphatase Stp1 mediates post-transcriptional regulation of hemolysin, autolysis, and virulence of group B *Streptococcus*. J Biol Chem 286:44197–44210. https://doi.org/10.1074/jbc.M111.313486
21. Cameron DR, Ward DV, Kostoulias X, Howden BP, Moellering Jr RC, Eliopoulos GM, Peleg AY (2012) Serine/threonine phosphatase Stp1 contributes to reduced susceptibility to vancomycin and virulence in *Staphylococcus aureus*. J Infect Dis 205:1677–1687. https://doi.org/10.1093/infdis/jis252
22. Zheng WH, Cai XD, Xie MS, Liang YJ, Wang T, Li ZG (2016) Structure-based identification of a potent inhibitor targeting Stp1-mediated virulence regulation in *Staphylococcus aureus*. Cell Chem Biol 23:1002–1013. https://doi.org/10.1016/j.chembiol.2016.06.014
23. Liu T-t, Yang T, Gao M-n, Chen K-x, Yang S, Yu K-q, Jiang H-l (2019) The inhibitory mechanism of aurintricarboxylic acid targeting serine/threonine phosphatase Stp1 in *Staphylococcus aureus*: insights from molecular dynamics simulations. Acta Pharmacol Sin 40:850–858. https://doi.org/10.1038/s41401-019-0216-x
24. Murthy HN, Kim YS, Park SY, Paek KY (2014) Biotechnological production of caffeic acid derivatives from cell and organ cultures of Echinacea species. Appl Microbiol Biotechnol 98:7707–7717. https://doi.org/10.1007/s00253-014-5962-6
25. Chen W, Lin H-R, Wei C-M, Luo X-H, Sun M-L, Yang Z-Z, Chen X-Y, Wang H-B (2018) Echinacoside, a phenylethanoid glycoside from Cistanche deserticola, extends lifespan of Caenorhabditis elegans and protects from Aβ-induced toxicity. Biogerontology 19:47–65. https://doi.org/10.1007/s10522-017-9738-0
26. Xiong WT, Gu L, Wang C, Sun HX, Liu X (2013) Anti-hyperglycemic and hypolipidemic effects of Cistanche tubulosa in type 2 diabetic db/db mice. J Ethnopharmacol 150:935–945. https://doi.org/10.1016/j.jep.2013.09.027
27. Macková A, Mucaji P, Widowitz U, Bauer R (2013) In vitro anti-inflammatory activity of Ligustrum vulgare extracts and their analytical characterization. Nat Prod Commun 8:1509–1512. https://doi.org/10.1177/1934578X1300801102
28. Dong L, Yu D, Wu N, Wang H, Niu J, Wang Y, Zou Z (2015) Echinacoside induces apoptosis in human SW480 colorectal cancer cells by induction of oxidative DNA damages. Int J Mol Sci 16:14655–14668. https://doi.org/10.3390/ijms160714655
29. Chuang HW, Wang TY, Huang CC, Wei IH (2022) Echinacoside exhibits antidepressant-like effects through AMPAR-Akt/ERK-mTOR pathway stimulation and BDNF expression in mice. Chin Med 17:1–12. https://doi.org/10.1186/s13020-021-00549-5
30. Yang Y, Wang X, Gao Y, Wang H, Niu X (2021) Insight into the dual inhibitory mechanism of verbascoside targeting serine/threonine phosphatase Stp1 against *Staphylococcus aureus*. Eur J Pharm Sci 157:1–11. https://doi.org/10.1016/j.ejps.2020.105628
31. Gao YW, Wang HS, Li XN, Niu XD (2023) Molecular mechanism of green tea polyphenol epicatechin gallate attenuating *Staphylococcus aureus* pathogenicity by targeting Ser/Thr phosphatase Stp1. Food Funct 14:4792–4806. https://doi.org/10.1039/d3fo00170a
32. Song M, Li L, Li M, Cha YH, Deng XM, Wang JF (2016) Apigenin protects mice from *pneumococcal* pneumonia by inhibiting the cytolytic activity of pneumolysin. Fitoterapia 115:31–36. https://doi.org/10.1016/j.fitote.2016.09.017
33. Teng Z, Shi D, Liu H, Shen Z, Zha Y, Li W, Deng X, Wang J (2017) Lysionotin attenuates *Staphylococcus aureus* pathogenicity by inhibiting alpha-toxin expression. Appl Microbiol Biotechnol 101:6697–6703. https://doi.org/10.1007/s00253-017-8417-z
34. Vieira TF, Sousa SF (2019) Comparing AutoDock and Vina in ligand/decoy discrimination for virtual screening. Appl Sci 9:1–18. https://doi.org/10.3390/app9214538
35. Fuhrmann J, Rurainski A, Lenhof HP, Neumann D (2010) A new Lamarckian genetic algorithm for flexible ligand-receptor docking. J Comput Chem 31:1911–1918. https://doi.org/10.1002/jcc.21478
36. Zayed MF, Ibrahim SRM, Habib ESE, Hassan MH, Ahmed S, Rateb HS (2019) Design, synthesis, antimicrobial and anti-biofilm evaluation, and molecular docking of newly substituted

fluoroquinazolinones. Med Chem 15:659–675. https://doi.org/10.2174/1573406414666181109092944
37. Wang X, Yang Y, Gao Y, Niu X (2020) Discovery of the novel inhibitor against New Delhi metallo-β-lactamase based on virtual screening and molecular modelling. Int J Mol Sci 21:1–14. https://doi.org/10.3390/ijms21103567
38. Nhung NT, Duong N, Phung HTT, Vo QV, Tam NM (2022) In silico screening of potential β-secretase (BACE1) inhibitors from VIETHERB database. J Mol Model 28:1–10. https://doi.org/10.1007/s00894-022-05051-9
39. Panteva MT, Giambasu GM, York DM (2015) Force field for Mg^{2+}, Mn^{2+}, Zn^{2+}, and Cd^{2+} ions that have balanced interactions with nucleic acids. J Phys Chem B 119:15460–15470. https://doi.org/10.1021/acs.jpcb.5b10423
40. Zarezade V, Abolghasemi M, Rahim F, Veisi A, Behbahani M (2018) In silico assessment of new progesterone receptor inhibitors using molecular dynamics: a new insight into breast cancer treatment. J Mol Model 24:1–19. https://doi.org/10.1007/s00894-018-3858-6
41. Eftink MR, Ghiron CA (1981) Fluorescence quenching studies with proteins. Anal Biochem 114:199–227. https://doi.org/10.1016/0003-2697(81)90474-7
42. Daina A, Michielin O, Zoete V (2017) SwissADME: a free web tool to evaluate pharmacokinetics, drug-likeness and medicinal chemistry friendliness of small molecules. Sci Rep 7:1–13. https://doi.org/10.1038/srep42717
43. Çalışkaner ZO (2022) Computational discovery of novel inhibitory candidates targeting versatile transcriptional repressor MBD2. J Mol Model 28:1–17. https://doi.org/10.1007/s00894-022-05297-3
44. Singh V, Dhankhar P, Dalal V, Tomar S, Golemi-Kotra D, Kumar P (2022) Drug-repurposing approach to combat *Staphylococcus aureus*: biomolecular and binding interaction study. ACS Omega 7:38448–38458. https://doi.org/10.1021/acsomega.2c03671
45. Yang T, Liu T, Gan J, Yu K, Chen K, Xue W, Lan L, Yang S, Yang C-G (2019) Structural insight into the mechanism of *Staphylococcus aureus* Stp1 phosphatase. ACS Infect Dis 5:841–850. https://doi.org/10.1021/acsinfecdis.8b00316
46. Liu J, Yang L, Dong Y, Zhang B, Ma X (2018) Echinacoside, an inestimable natural product in treatment of neurological and other disorders. Molecules 23:1–23. https://doi.org/10.3390/molecules23051213
47. Li F, Yang X, Yang Y, Li P, Yang Z, Zhang C (2015) Phospholipid complex as an approach for bioavailability enhancement of echinacoside. Drug Dev Ind Pharm 41:1777–1784. https://doi.org/10.3109/03639045.2015.1004183
48. Shen JY, Yang XL, Yang ZL, Kou JP, Li F (2015) Enhancement of absorption and bioavailability of echinacoside by verapamil or clove oil. Drug Des Devel Ther 9:4685–4693. https://doi.org/10.2147/dddt.s87581
49. Yang X, Li F, Yang Y, Shen J, Zou R, Zhu P, Zhang C, Yang Z, Li P (2013) Efficacy and safety of echinacoside in a rat osteopenia model. Evid Based Complement Alternat Med 2013:1–11. https://doi.org/10.1155/2013/926928
50. Wu Y, Li L, Wen T, Li Y-Q (2007) Protective effects of echinacoside on carbon tetrachloride-induced hepatotoxicity in rats. Toxicology 232:50–56. https://doi.org/10.1016/j.tox.2006.12.013